Supplementary Material for From Nodal Chain Semimetal To Weyl Semimetal in HfC

Rui Yu[1],* Quansheng Wu[2], Zhong Fang[3,4], and Hongming Weng[3,4]†
[1] *School of Physics and Technology, Wuhan University, Wuhan 430072, China*
[2] *Theoretical Physics and Station Q Zurich, ETH Zurich, 8093 Zurich, Switzerland*
[3] *Beijing National Laboratory for Condensed Matter Physics, and Institute of Physics,Chinese Academy of Sciences, Beijing 100190, China and*
[4] *Collaborative Innovation Center of Quantum Matter, Beijing 100190, China*

The supplementary material is organized in the following manner. In section I, we present the bulk band structures checking with HSE and GGA+U calculations. In section II, we show how to construct the SOC Hamiltonians for the $k \cdot p$ models given in the main text and discuss the possibility of appearing of Weyl points in HfC with SOC. In section III, we present the Berry curvatures near the Weyl points, which are used to determine the chirality of the Weyl points. In section IV, we give the details for the Wannier-based tight-binding model and the surface states on the (100) surface.

I. THE BAND STRUCTURES FROM HSE AND LDA+U CALCULATIONS

To overcome possible overestimation of band inversion [1], we employed hybrid density functionals [2] to confirm the existence of band inversion. As shown in Fig. 1 (a), the red solid bands are calculated by GGA without the SOC while the blue dashed bands are calculated by HSE. We also performed the GGA+U calculation to confirm the nonmagnetic phase of HfC. We find the band structure is insensitive to the typical value of U and J for 5d electrons as shown in Fig. 1 (b), where the red solid band are calculated with $U = 2, J = 0.4$ and the blue dashed bands are calculated with $U = 4, J = 0.8$, respectively.

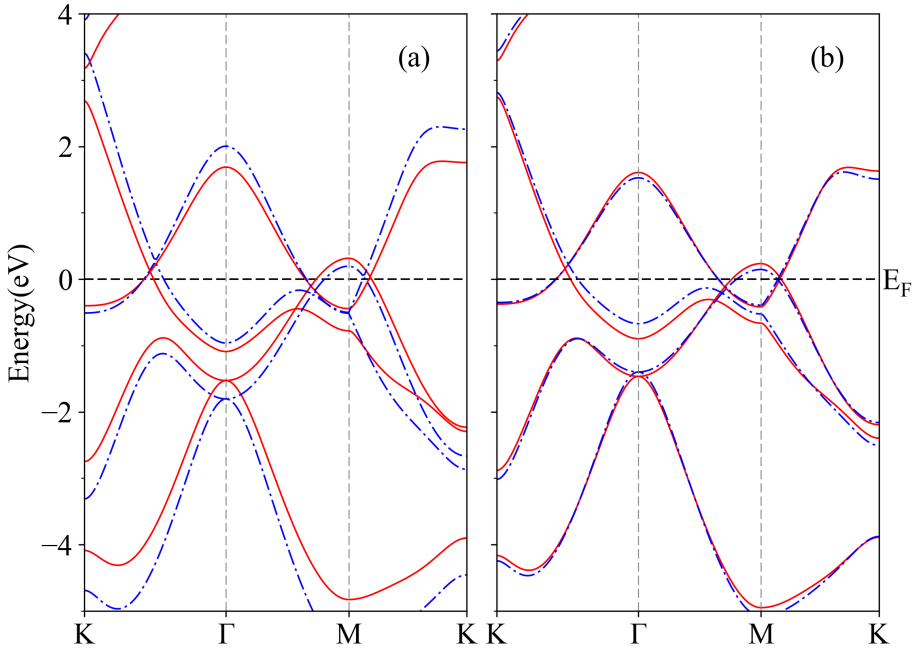

Figure 1. (Color online) (a) The band structure of HfC calculated by GGA (red solid bands) and HSE06 (blue dashed bands) without including the SOC. (b) The band structure of HfC calculated by GGA+U with $U = 2, J = 0.4$ (red solid bands) and $U = 4, J = 0.8$ (blue dashed bands).

* yurui1983@foxmail.com
† hmweng@iphy.ac.cn

II. THE SOC EFFECTIVE HAMILTONIAN AND THE POSSIBILITY OF APPEARING OF WEYL POINTS

In general, the SOC in the Pauli equation can be written as

$$H_{so} = \frac{\hbar}{4m_0^2c^2}(\nabla V \times \boldsymbol{p})\cdot \boldsymbol{\sigma} = \frac{\hbar}{4m_0^2c^2}(\boldsymbol{p}\times\boldsymbol{F})\cdot\boldsymbol{\sigma}, \tag{1}$$

where $\boldsymbol{p}$ is the momentum, V is the potential energy, $F \equiv -\nabla V$ is the force and $\boldsymbol{\sigma}$ are the Pauli matrices. We consider the nearest-neighbor SOC, which can be expressed in the following formula [3, 4]

$$H_{so} = \sum_{\langle ij\rangle\alpha\beta} i\gamma_{ij}c^{\dagger}_{i\alpha}(\boldsymbol{d}_{ij}\times\boldsymbol{F}_{ij})\cdot\boldsymbol{\sigma}_{\alpha\beta}c_{j\beta}, \tag{2}$$

where $\boldsymbol{d}_{ij}$ is the vector connect site i and j, γ_{ij} are undetermined parameters. There are 6 nearest C atoms surround Hf atom as shown in Fig. 2. Due to the mirror symmetry M_y, force F_{Hf,C_1} is parallel with the mirror plane as shown in Fig. 2 (b). The other force F_{Hf,C_i} $(i = 2, ..., 6)$ can be obtained by considering the C_3 and M_z symmetries of the HfC lattice.

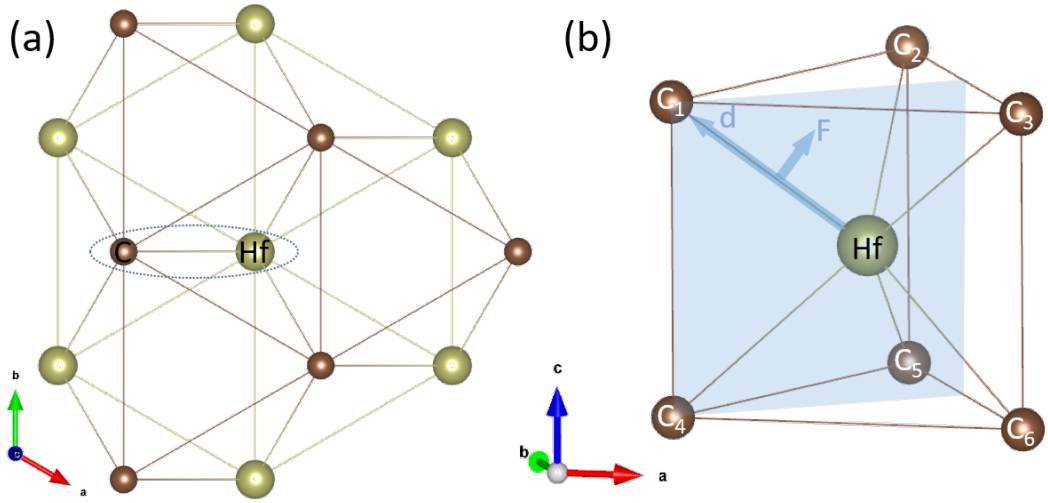

Figure 2. (Color online) (a) Top view and (b) side view of the HfC crystal structure. The force between Hf-C_1 is parallel with the mirror plane M_y (light blue plane in (b)).

We first consider the effective SOC Hamiltonian for the nodal ring states near Γ point. The two crossing states are mainly from d_{xy}-orbitals of Hf and p_z-orbitals of C. By performing Fourier transformations, we obtain the effective Hamiltonian

$$\begin{aligned} H^{\Gamma}_{so}(\boldsymbol{k}) =& i\lambda_{so}c^{\dagger}_{d_{xy}\alpha}(\boldsymbol{k})\Big((\frac{\sqrt{3}}{2}\sigma_x - \frac{1}{2}\sigma_y)e^{i\boldsymbol{k}\cdot(a+b)} - (-\frac{\sqrt{3}}{2}\sigma_x - \frac{1}{2}\sigma_y)e^{i\boldsymbol{k}\cdot a} \\ & - (-\frac{\sqrt{3}}{2}\sigma_x + \frac{1}{2}\sigma_y)e^{i\boldsymbol{k}\cdot(a+b-c)} + (\frac{\sqrt{3}}{2}\sigma_x + \frac{1}{2}\sigma_y)e^{i\boldsymbol{k}\cdot(a-c)}\Big)c_{p_z\beta}(\boldsymbol{k}) + h.c. \end{aligned} \tag{3}$$

around the Γ point in the basis $\{|d_{xy}\rangle, |p_z\rangle\} \otimes \{\uparrow, \downarrow\}$ from the symmetry aspect analysis. λ_{so} is the SOC parameter, a, b, c are the lattice vectors. The overlap integrals between Hf d_{xy}-orbital and C p_z-orbital are vanish along Hf-C_1 and Hf-C_4 neighbors, therefore the SOC only contributed from Hf-C_i $(i = 2, 3, 5, 6)$ neighbors. The above SOC Hamiltonian can be written in a compact form as

$$\mathcal{H}^{\Gamma}_{so}(\boldsymbol{k}) = \sum_{i,j=1,2} f_{ij}(\boldsymbol{k})\tau_i \otimes \sigma_j, \tag{4}$$

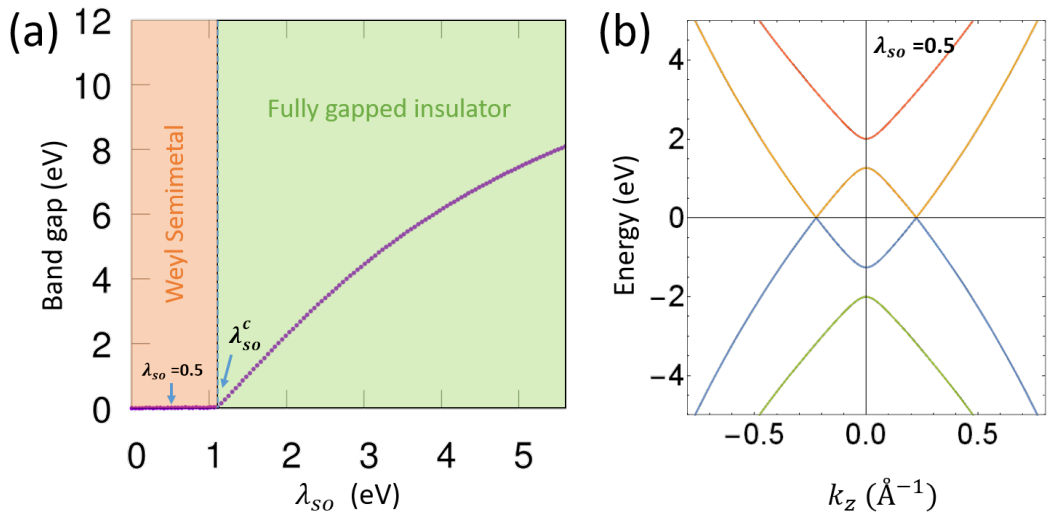

Figure 3. (Color online) (a) The band gap, $min[E_1(\mathbf{k}) - E_2(\mathbf{k})]$ as a function of λ_{so}. The gap closing points, i.e., Weyl points, exist for $\lambda_{so} < \lambda_{so}^c$. The band gap opens for $\lambda_{so} > \lambda_{so}^c$. The results are obtained by assuming $d_x = c_x k_y k_z$ and $d_y = c_y k_x k_y k_z$, which satisfy the symmetry constraints of time-reversal symmetry and mirror symmetries as discussed in the main text. The parameters $c_x = 8.9$ eV·Å^2 and $c_y = 4.6$ eV·Å^3 are obtained by fitting with the band dispersions from first-principle calculations. (b) The band dispersions along k_z crossing two Weyl points with opposite chirality in the case of $\lambda_{so} = 0.5$ eV marked in (a) and the position of one Weyl point is at (0.011, 0.777, 0.224) Å^{-1}.

where

$$
\begin{aligned}
f_{11} &= -2\sqrt{3}\lambda_{so} cos\frac{k_y}{2} cos\frac{k_z}{2} sin(\frac{\sqrt{3}k_x - k_z}{2}),\\
f_{21} &= -2\sqrt{3}\lambda_{so} cos\frac{k_y}{2} cos\frac{k_z}{2} cos(\frac{\sqrt{3}k_x - k_z}{2}),\\
f_{12} &= +2\lambda_{so} sin\frac{k_y}{2} cos\frac{k_z}{2} cos(\frac{\sqrt{3}k_x - k_z}{2}),\\
f_{22} &= -2\lambda_{so} sin\frac{k_y}{2} cos\frac{k_z}{2} sin(\frac{\sqrt{3}k_x - k_z}{2}).
\end{aligned}
\tag{5}
$$

Following the similar arguments, we can obtain the effective SOC Hamiltonian for the nodal line states near M point, which has the same formula as expressed in Eq. 4 and Eq. 5.

The appearance of Weyl points can also be derived from the $\boldsymbol{k}\cdot\boldsymbol{p}$ models Eq. 1 and Eq. 9 in the main text with the spin-orbit interactions given in Eq. 4. Here we discuss the Weyl points decay from the nodal ring surrounding Γ point. The effective Hamiltonian with SOC is given as

$$
H(\boldsymbol{k}) = H_0^{\Gamma}(\boldsymbol{k}) + H_{so}^{\Gamma}(\boldsymbol{k}),
\tag{6}
$$

where $H_0^{\Gamma}(\boldsymbol{k})$ is given in Eq. 1 in the main text. The dispersion with the SOC terms are $E_{1,2}(\boldsymbol{k}) = \pm\sqrt{d^2(\boldsymbol{k}) + f^2(\boldsymbol{k}) - q(\boldsymbol{k})}$ and $E_{3,4}(\boldsymbol{k}) = \pm\sqrt{d^2(\boldsymbol{k}) + f^2(\boldsymbol{k}) + q(\boldsymbol{k})}$, where $d^2 = d_x^2(\boldsymbol{k}) + d_y^2(\boldsymbol{k}) + d_z^2(\boldsymbol{k})$, $f^2 = f_{11}^2(\boldsymbol{k}) + f_{12}^2(\boldsymbol{k}) + f_{21}^2(\boldsymbol{k}) + f_{22}^2(\boldsymbol{k})$ and $q(\boldsymbol{k}) = 2[2(f_{11}f_{12} + f_{21}f_{22})d_x d_y + (f_{11}^2 + f_{21}^2)d_x^2 + (f_{12}^2 + f_{22}^2)d_y^2 + (f_{12}f_{21} - f_{11}f_{22})^2]^{1/2}$. The Weyl points appear if the $E_{1,2}(\boldsymbol{k}) = 0$ are satisfied. In the following discussions, we focus on the solutions with $k_y > 0$ and $k_z > 0$. With some straightforward algebraic derivation, $E_{1,2}^2(\boldsymbol{k})$ are simplified as

$$
E_1^2(\boldsymbol{k}) = d^2 + 8\lambda_{so}^2 cos^2\frac{k_z}{2} + \lambda_{so}^2 C(\boldsymbol{k}) cos^2\frac{k_z}{2} cos(k_y + \beta(\boldsymbol{k})),
\tag{7}
$$

where $C(\boldsymbol{k}) = 4\sqrt{1 + 3\Delta(\boldsymbol{k})}$, $\Delta(\boldsymbol{k})$=1+$(3d_x^2(1+cosk_y)+d_y^2(1-cosk_y))/(6\lambda_{so}^2 sin^2 k_y cos^2\frac{k_z}{2})$, and $\beta(\boldsymbol{k})$=$arcsin\frac{4\sqrt{3\Delta(\boldsymbol{k})}}{C(\boldsymbol{k})}$. It can be shown that the equation $E_{1,2}(\boldsymbol{k}) = 0$ is equivalent to the following equation:

$$
cos(k_y + \beta) = -\frac{d^2(\boldsymbol{k}) + 8\lambda_{so}^2 cos^2\frac{k_z}{2}}{\lambda_{so}^2 C(\boldsymbol{k}) cos^2\frac{k_z}{2}}.
\tag{8}
$$

On the $k_z = 0$ plane, we have $d_{x,y} = 0$ as indicated in Eq. 5 of main text. Therefore Eq. 8 is simplified to

$$cos(k_y + \frac{\pi}{3}) = -(1 + \frac{d_z(\boldsymbol{k})^2}{8\lambda_{so}^2}). \tag{9}$$

Eq. 9 is satisfied if $d_z(\boldsymbol{k}) = 0$ and $k_y = \frac{2\pi}{3} + 2n\pi, (n = 0, 1, 2, ...)$. This solution exists only if the nodal ring on the $k_z = 0$ plane crosses the line determined by $k_y = \frac{2\pi}{3} + 2n\pi$. But it is not satisfied in the HfC system. Therefore, there is no Weyl points on the $k_z = 0$ plane. Away from the $k_z = 0$ plane, it is difficult to solve Eq. 8 analytically. However, the formula of Eq. 8 shows that there is the possibility of finding solutions that make the absolute value of the right hand side less than one and equals to $cos(k_y + \beta)$ simultaneously. Therefore the Weyl points can appear away from the $k_z = 0$ plane. Numerically solving Eq. 7, we find Weyl points exist for $\lambda_{so} < \lambda_{so}^c$ as shown in Fig. 3. For $\lambda_{so} > \lambda_{so}^c$, the gap opens and the system becomes an insulator. This result indicates that the effective SOC in HfC is relatively weak and makes it in phase with Weyl points. By performing the first-principles calculation, we find 6 pairs of Weyl point away from $k_z = 0$ plane. Following the similar argument, we can find that the SOC will gap the nodal ring on $k_y = 0$ plane, and as a consequence, the Weyl points can appear away from $k_y = 0$ plane.

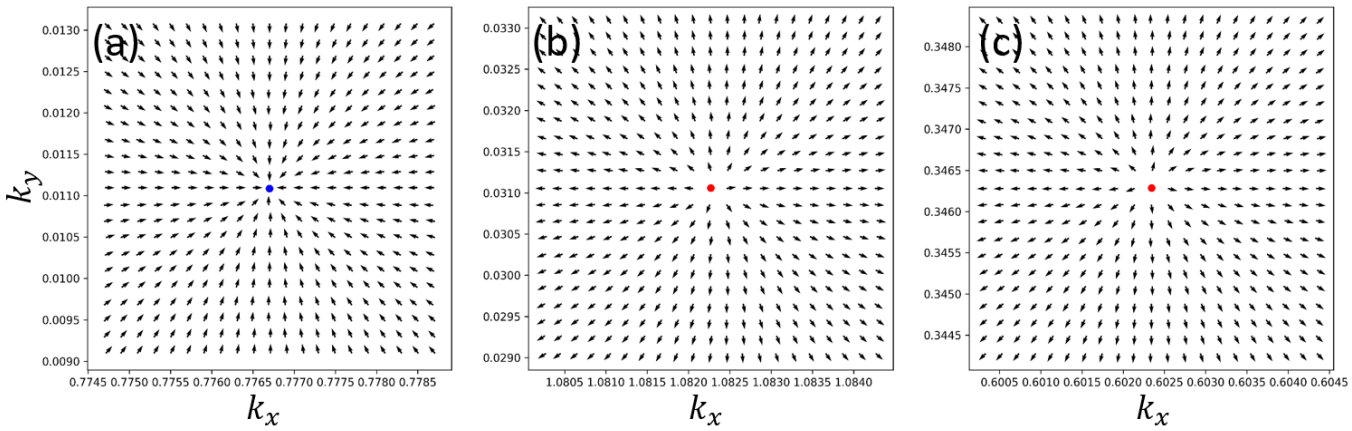

Figure 4. (Color online) The distribution of the Berry curvature on the k_x-k_y plane that pass through the Weyl point. (a) for W_1 type of Weyl point with chirality $\chi = -1$, (b) for W_2 type of Weyl point with chirality $\chi = +1$ and (c) for W_3 type of Weyl point with chirality $\chi = +1$.

III. BERRY CURVATURE NEAR WEYL POINTS

In order to determine precisely the location of the Weyl points, we divide the BZ into a very dense k-point mesh and compute the Berry curvature or the 'magnetic filed in momentum space' for the low branch in the Weyl cone. The position for the $W_{1,2,3}$ type of Weyl points are listed in Tab. I in the main text. The chirality of the Weyl point can be determined by checking the configuration of the 'magnetic filed in momentum space'. The 'source' ('drain') points of the 'magnetic filed' indicate the Weyl points with chirality $\chi = +1$ (-1). The distribution of the Berry curvature near the $W_{1,2,3}$ type of Weyl points are shown in Fig. 4, where the red and blue dots denote the Weyl points with chirality of $+1$ and -1, respectively.

IV. BULK BANDS AND SURFACE BANDS CALCULATED WITH WANNIER-BASED TIGHT-BINDING MODEL

The tight-binding model of the 2p-orbitals of C and 5d-orbitals of Hf has been constructed based on the maximally localized Wannier functions (MLWFs) [5]. As shown in Fig. 5, for HfC without and with SOC, the band structures obtained from the Wannier-based tight-binding Hamiltonian (red solid lines) almost exactly reproduce the *ab initio* band structures (blue dashed lines). The surface states for a semi-infinite slab along the (001) direction are calculated by using these Hamiltonians and shown in Fig. 6 (a) without and (b) with SOC. The Fermi surface for (001) surface are given in the main text. The surface states for (100) surface are much more complicated, as shown in Fig. 7 (a).

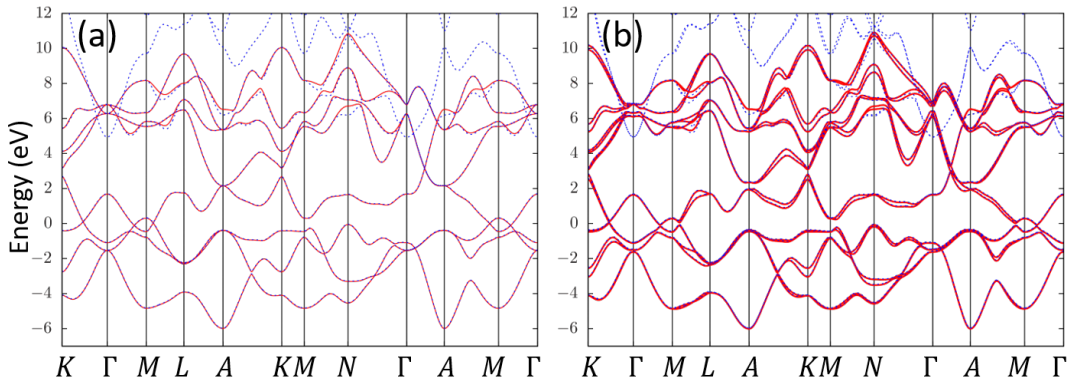

Figure 5. (Color online) Comparison of bands calculated with Wannier-based tight-binding model (red solid lines) with the *ab initio* band structures (blue dashed lines) of HfC (a) without SOC and (b) with SOC. The Wannier-based tight-binding model almost exactly reproduces the *ab initio* band structures.

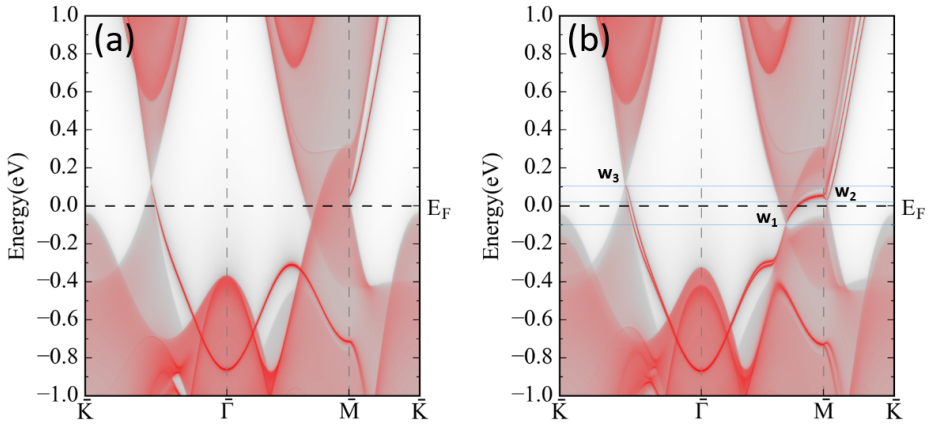

Figure 6. (Color online) The (001) surface states (a) without and (b) with SOC are calculated by using the Wannier-based tight-binding Hamiltonian. The surface states are split after including SOC and connect to the projected Weyl point on the surface.

For the Weyl points are covered with the bulk states, it is not easy to see how the Fermi arcs are connected to the projections of the Wey points on (100) surfaces.

[1] J. Vidal, X. Zhang, L. Yu, J.-W. Luo, and A. Zunger, Phys. Rev. B **84**, 041109 (2011).
[2] J. Heyd, G. E. Scuseria, and M. Ernzerhof, The Journal of Chemical Physics **118**, 8207 (2003).
[3] C. L. Kane and E. J. Mele, Phys. Rev. Lett. **95** (2005).
[4] C.-C. Liu, H. Jiang, and Y. Yao, Phys. Rev. B **84** (2011).
[5] N. Marzari, A. A. Mostofi, J. R. Yates, I. Souza, and D. Vanderbilt, Rev. Mod. Phys. **84**, 1419 (2012).

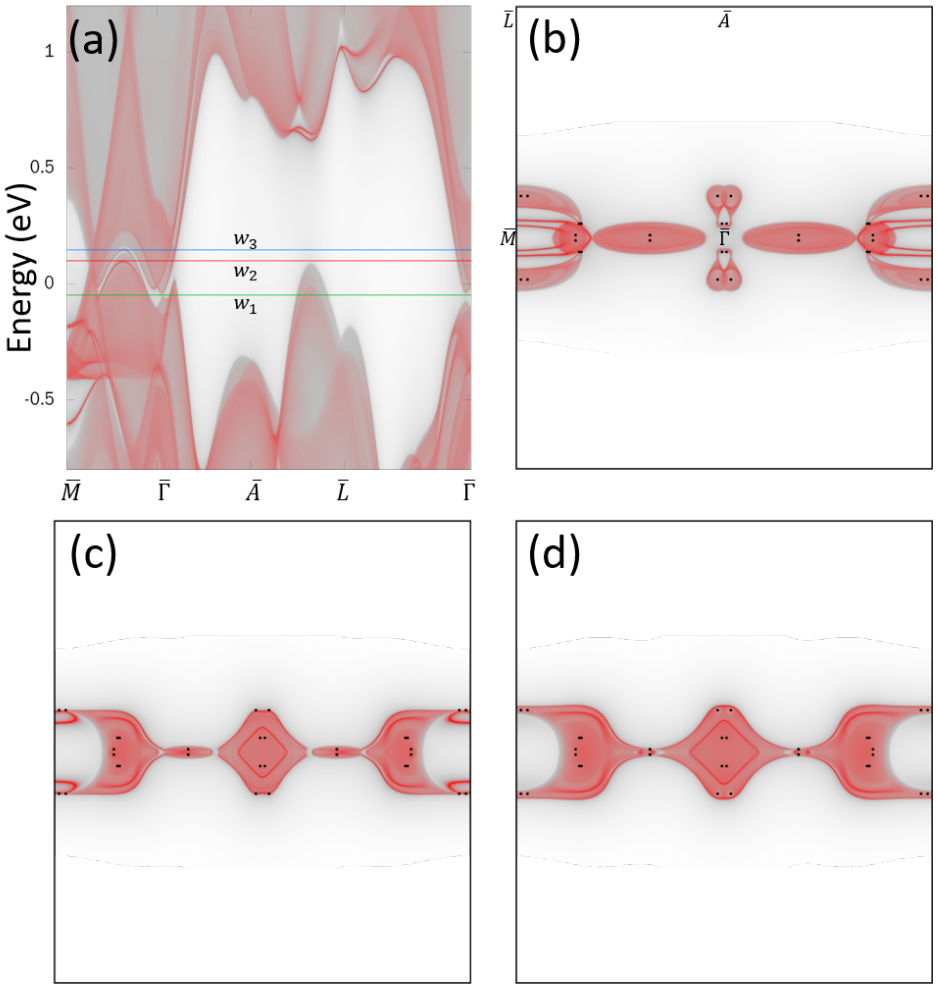

Figure 7. (Color online) (a) Surface states of HfC terminated in (100) direction. (b-d) Fermi surface of HfC (100)-surface states. Chemical potential is set at (b) W_1, (c) W_2, and (d) W_3 type of Weyl point.